EUROPEAN ORGANIZATION FOR NUCLEAR RESEARCH

CERN-PPE/94-201
1st December 1994

Inclusive $\pi^{\pm}$, $K^{\pm}$ and $(p, \bar{p})$ Differential Cross-sections at the Z Resonance.

The **ALEPH** Collaboration [1]

Abstract

Inclusive $\pi^{\pm}$, $K^{\pm}$ and $(p, \bar{p})$ differential cross-sections in hadronic decays of the Z have been measured as a function of $z = p_{\rm hadron}/p_{\rm beam}$, the scaled momentum. The results are based on approximately 520 000 events measured by the ALEPH detector at LEP during 1992. Charged particles are identified by their rate of ionization energy loss in the ALEPH Time Projection Chamber. The position, $\xi^{\star}$, of the peak in the $\ln(1/z)$ distribution is determined, and the evolution of the peak position with centre-of-mass energy is compared with the prediction of QCD.

(Submitted to Zeitschrift für Physik.)

[1] See following pages for list of authors.

The ALEPH Collaboration

D. Buskulic, D. Casper, I. De Bonis, D. Decamp, P. Ghez, C. Goy, J.-P. Lees, M.-N. Minard, P. Odier, B. Pietrzyk

Laboratoire de Physique des Particules (LAPP), IN^{2}P^3-CNRS, 74019 Annecy-le-Vieux Cedex, France

F. Ariztizabal, M. Chmeissani, J.M. Crespo, I. Efthymiopoulos, E. Fernandez, M. Fernandez-Bosman, V. Gaitan, Ll. Garrido,[15] M. Martinez, S. Orteu, A. Pacheco, C. Padilla, F. Palla, A. Pascual, J.A. Perlas, F. Sanchez, F. Teubert

Institut de Fisica d'Altes Energies, Universitat Autonoma de Barcelona, 08193 Bellaterra (Barcelona), Spain[7]

D. Creanza, M. de Palma, A. Farilla, G. Iaselli, G. Maggi, N. Marinelli, S. Natali, S. Nuzzo, A. Ranieri, G. Raso, F. Romano, F. Ruggieri, G. Selvaggi, L. Silvestris, P. Tempesta, G. Zito

Dipartimento di Fisica, INFN Sezione di Bari, 70126 Bari, Italy

X. Huang, J. Lin, Q. Ouyang, T. Wang, Y. Xie, R. Xu, S. Xue, J. Zhang, L. Zhang, W. Zhao

Institute of High-Energy Physics, Academia Sinica, Beijing, The People's Republic of China[8]

G. Bonvicini, M. Cattaneo, P. Comas, P. Coyle, H. Drevermann, A. Engelhardt, R.W. Forty, M. Frank, G. Ganis, C. Gay,[3] M. Girone, R. Hagelberg, J. Harvey, R. Jacobsen, B. Jost, J. Knobloch, I. Lehraus, M. Maggi, C. Markou, E.B. Martin, P. Mato, H. Meinhard, A. Minten, R. Miquel, P. Palazzi, J.R. Pater, P. Perrodo, J.-F. Pusztaszeri, F. Ranjard, L. Rolandi, D. Schlatter, M. Schmelling, W. Tejessy, I.R. Tomalin, R. Veenhof, A. Venturi, H. Wachsmuth, W. Wiedenmann, W. Witzeling, J. Wotschack

European Laboratory for Particle Physics (CERN), 1211 Geneva 23, Switzerland

Z. Ajaltouni, M. Bardadin-Otwinowska,[2] A. Barres, C. Boyer, A. Falvard, P. Gay, C. Guicheney, P. Henrard, J. Jousset, B. Michel, S. Monteil, J-C. Montret, D. Pallin, P. Perret, F. Podlyski, J. Proriol, J.-M. Rossignol, F. Saadi

Laboratoire de Physique Corpusculaire, Université Blaise Pascal, IN^{2}P^3-CNRS, Clermont-Ferrand, 63177 Aubière, France

T. Fearnley, J.B. Hansen, J.D. Hansen, J.R. Hansen, P.H. Hansen, S.D. Johnson, B.S. Nilsson

Niels Bohr Institute, 2100 Copenhagen, Denmark[9]

A. Kyriakis, E. Simopoulou, I. Siotis, A. Vayaki, K. Zachariadou

Nuclear Research Center Demokritos (NRCD), Athens, Greece

A. Blondel, G. Bonneaud, J.C. Brient, P. Bourdon, L. Passalacqua, A. Rougé, M. Rumpf, R. Tanaka, A. Valassi, M. Verderi, H. Videau

Laboratoire de Physique Nucléaire et des Hautes Energies, Ecole Polytechnique, IN^{2}P^3-CNRS, 91128 Palaiseau Cedex, France

D.J. Candlin, M.I. Parsons, E. Veitch

Department of Physics, University of Edinburgh, Edinburgh EH9 3JZ, United Kingdom[10]

E. Focardi, G. Parrini

Dipartimento di Fisica, Università di Firenze, INFN Sezione di Firenze, 50125 Firenze, Italy

M. Corden, M. Delfino,[12] C. Georgiopoulos, D.E. Jaffe

Supercomputer Computations Research Institute, Florida State University, Tallahassee, FL 32306-4052, USA [13,14]

A. Antonelli, G. Bencivenni, G. Bologna,[4] F. Bossi, P. Campana, G. Capon, F. Cerutti, V. Chiarella, G. Felici, P. Laurelli, G. Mannocchi,[5] F. Murtas, G.P. Murtas, M. Pepe-Altarelli, S. Salomone

Laboratori Nazionali dell'INFN (LNF-INFN), 00044 Frascati, Italy

P. Colrain, I. ten Have,[6] I.G. Knowles, J.G. Lynch, W. Maitland, W.T. Morton, C. Raine, J.M. Scarr, K. Smith, M.G. Smith, A.S. Thompson, S. Thorn, R.M. Turnbull

Department of Physics and Astronomy, University of Glasgow, Glasgow G12 8QQ, United Kingdom[10]

U. Becker, O. Braun, C. Geweniger, G. Graefe, P. Hanke, V. Hepp, E.E. Kluge, A. Putzer, B. Rensch, M. Schmidt, J. Sommer, H. Stenzel, K. Tittel, M. Wunsch

Institut für Hochenergiephysik, Universität Heidelberg, 69120 Heidelberg, Fed. Rep. of Germany[16]

R. Beuselinck, D.M. Binnie, W. Cameron, D.J. Colling, P.J. Dornan, N. Konstantinidis, L. Moneta, A. Moutoussi, J. Nash, G. San Martin, J.K. Sedgbeer, A.M. Stacey

Department of Physics, Imperial College, London SW7 2BZ, United Kingdom[10]

G. Dissertori, P. Girtler, E. Kneringer, D. Kuhn, G. Rudolph

Institut für Experimentalphysik, Universität Innsbruck, 6020 Innsbruck, Austria[18]

C.K. Bowdery, T.J. Brodbeck, A.J. Finch, F. Foster, G. Hughes, D. Jackson, N.R. Keemer, M. Nuttall, A. Patel, T. Sloan, S.W. Snow, E.P. Whelan

Department of Physics, University of Lancaster, Lancaster LA1 4YB, United Kingdom[10]

A. Galla, A.M. Greene, K. Kleinknecht, J. Raab, B. Renk, H.-G. Sander, H. Schmidt, S.M. Walther, R. Wanke, B. Wolf

Institut für Physik, Universität Mainz, 55099 Mainz, Fed. Rep. of Germany[16]

J.J. Aubert, A.M. Bencheikh, C. Benchouk, A. Bonissent, G. Bujosa, D. Calvet, J. Carr, C. Diaconu, F. Etienne, M. Thulasidas, D. Nicod, P. Payre, D. Rousseau, M. Talby

Centre de Physique des Particules, Faculté des Sciences de Luminy, IN^{2}P^3-CNRS, 13288 Marseille, France

I. Abt, R. Assmann, C. Bauer, W. Blum, D. Brown, H. Dietl, F. Dydak,[21] C. Gotzhein, A.W. Halley, K. Jakobs, H. Kroha, G. Lütjens, G. Lutz, W. Männer, H.-G. Moser, R. Richter, A. Rosado-Schlosser, A.S. Schwarz,[23] R. Settles, H. Seywerd, U. Stierlin,[2] R. St. Denis, G. Wolf

Max-Planck-Institut für Physik, Werner-Heisenberg-Institut, 80805 München, Fed. Rep. of Germany[16]

R. Alemany, J. Boucrot, O. Callot, A. Cordier, F. Courault, M. Davier, L. Duflot, J.-F. Grivaz, Ph. Heusse, M. Jacquet, P. Janot, D.W. Kim,[19] F. Le Diberder, J. Lefrançois, A.-M. Lutz, G. Musolino, I. Nikolic, H.J. Park, I.C. Park, M.-H. Schune, S. Simion, J.-J. Veillet, I. Videau

Laboratoire de l'Accélérateur Linéaire, Université de Paris-Sud, IN^{2}P^3-CNRS, 91405 Orsay Cedex, France

D. Abbaneo, G. Bagliesi, G. Batignani, S. Bettarini, U. Bottigli, C. Bozzi, G. Calderini, M. Carpinelli, M.A. Ciocci, V. Ciulli, R. Dell'Orso, I. Ferrante, F. Fidecaro, L. Foà,[1] F. Forti, A. Giassi, M.A. Giorgi, A. Gregorio, F. Ligabue, A. Lusiani, P.S. Marrocchesi, A. Messineo, G. Rizzo, G. Sanguinetti, A. Sciabà, P. Spagnolo, J. Steinberger, R. Tenchini, G. Tonelli,[26] G. Triggiani, C. Vannini, P.G. Verdini, J. Walsh

Dipartimento di Fisica dell'Università, INFN Sezione di Pisa, e Scuola Normale Superiore, 56010 Pisa, Italy

A.P. Betteridge, G.A. Blair, L.M. Bryant, Y. Gao, M.G. Green, D.L. Johnson, T. Medcalf, Ll.M. Mir, J.A. Strong

Department of Physics, Royal Holloway & Bedford New College, University of London, Surrey TW20 OEX, United Kingdom[10]

V. Bertin, D.R. Botterill, R.W. Clifft, T.R. Edgecock, S. Haywood, M. Edwards, P. Maley, P.R. Norton, J.C. Thompson

Particle Physics Dept., Rutherford Appleton Laboratory, Chilton, Didcot, Oxon OX11 OQX, United Kingdom[10]

B. Bloch-Devaux, P. Colas, H. Duarte, S. Emery, W. Kozanecki, E. Lançon, M.C. Lemaire, E. Locci, B. Marx, P. Perez, J. Rander, J.-F. Renardy, A. Rosowsky, A. Roussarie, J.-P. Schuller, J. Schwindling, D. Si Mohand, A. Trabelsi, B. Vallage

CEA, DAPNIA/Service de Physique des Particules, CE-Saclay, 91191 Gif-sur-Yvette Cedex, France[17]

R.P. Johnson, A.M. Litke, G. Taylor, J. Wear

Institute for Particle Physics, University of California at Santa Cruz, Santa Cruz, CA 95064, USA[22]

A. Beddall, C.N. Booth, R. Boswell, S. Cartwright, F. Combley, I. Dawson, A. Koksal, M. Letho, W.M. Newton, C. Rankin, P. Reeves,[27] L.F. Thompson

Department of Physics, University of Sheffield, Sheffield S3 7RH, United Kingdom[10]

A. Böhrer, S. Brandt, G. Cowan, E. Feigl, C. Grupen, G. Lutters, J. Minguet-Rodriguez, F. Rivera,[25] P. Saraiva, U. Schäfer, L. Smolik

Fachbereich Physik, Universität Siegen, 57068 Siegen, Fed. Rep. of Germany[16]

L. Bosisio, R. Della Marina, G. Giannini, B. Gobbo, L. Pitis, F. Ragusa[20]

Dipartimento di Fisica, Università di Trieste e INFN Sezione di Trieste, 34127 Trieste, Italy

H. Kim, J. Rothberg, S. Wasserbaech

Experimental Elementary Particle Physics, University of Washington, WA 98195 Seattle, U.S.A.

S.R. Armstrong, L. Bellantoni, J.S. Conway,[24] P. Elmer, Z. Feng, D.P.S. Ferguson, Y.S. Gao, S. Gonzáles, J. Grahl, J.L. Harton, O.J. Hayes, H. Hu, P.A. McNamara III, J.M. Nachtman, W. Orejudos, Y.B. Pan, Y. Saadi, M. Schmitt, I.J. Scott, V. Sharma, J.D. Turk, A.M. Walsh, F.V. Weber,[1] T. Wildish, Sau Lan Wu, X. Wu, J.M. Yamartino, M. Zheng, G. Zobernig

Department of Physics, University of Wisconsin, Madison, WI 53706, USA[11]

---

[1] Now at CERN, 1211 Geneva 23, Switzerland.
[2] Deceased.
[3] Now at Harvard University, Cambridge, MA 02138, U.S.A.
[4] Also Istituto di Fisica Generale, Università di Torino, Torino, Italy.
[5] Also Istituto di Cosmo-Geofisica del C.N.R., Torino, Italy.
[6] Now at TSM Business School, Enschede, The Netherlands.
[7] Supported by CICYT, Spain.
[8] Supported by the National Science Foundation of China.
[9] Supported by the Danish Natural Science Research Council.
[10] Supported by the UK Science and Engineering Research Council.
[11] Supported by the US Department of Energy, contract DE-AC02-76ER00881.
[12] On leave from Universitat Autonoma de Barcelona, Barcelona, Spain.
[13] Supported by the US Department of Energy, contract DE-FG05-92ER40742.
[14] Supported by the US Department of Energy, contract DE-FC05-85ER250000.
[15] Permanent address: Universitat de Barcelona, 08208 Barcelona, Spain.
[16] Supported by the Bundesministerium für Forschung und Technologie, Fed. Rep. of Germany.
[17] Supported by the Direction des Sciences de la Matière, C.E.A.
[18] Supported by Fonds zur Förderung der wissenschaftlichen Forschung, Austria.
[19] Permanent address: Kangnung National University, Kangnung, Korea.
[20] Now at Dipartimento di Fisica, Università di Milano, Milano, Italy.
[21] Also at CERN, 1211 Geneva 23, Switzerland.
[22] Supported by the US Department of Energy, grant DE-FG03-92ER40689.
[23] Now at DESY, Hamburg, Germany.
[24] Now at Rutgers University, Piscataway, NJ 08854, USA.
[25] Partially supported by Colciencias, Colombia.
[26] Also at Istituto di Matematica e Fisica, Università di Sassari, Sassari, Italy.
[27] Now at University of Glasgow, Glasgow G12 8QQ, United Kingdom.

1 Introduction

A measurement of the composition of the hadronic final state in e^+e^- annihilation is fundamental to an understanding of the fragmentation of quarks and gluons into hadrons. While no calculable theory yet exists for this process, a number of phenomenological models have evolved, falling into two broad classes: "string" fragmentation and "cluster" fragmentation, as exemplified by the JETSET [1] and HERWIG [2] Monte Carlos, respectively.

In this letter, a measurement of the rates of $\pi^{\pm}$, $K^{\pm}$ and $(p, \bar{p})$ production in hadronic decays of the Z is presented as a function of $z = p_{\mathrm{hadron}}/p_{\mathrm{beam}}$, the scaled momentum. Particles are identified by a simultaneous measurement of their momentum and specific energy loss dE/dx. Differential cross-sections are compared with the predictions of the JETSET 7.3 and HERWIG 5.6 Monte Carlos. Recently a measurement was published by OPAL [3]. The position of the peak ξ^* in the $\ln(1/z)$ distribution is determined, and the evolution of the peak position with centre-of-mass energy is compared with the prediction of QCD.

The following sections describe the ALEPH detector, hadronic event selection and dE/dx measurement. A maximum-likelihood fit for the rates of pions, kaons and protons is presented. Finally, the results and errors are discussed.

2 The ALEPH detector and hadronic event selection

The ALEPH detector has been described in detail elsewhere [4]. Here the components relevant to the present analysis are reviewed. The momenta of charged particles are measured in three concentric tracking chambers: the principal detector is a time projection chamber (TPC) of radius 1.8 m and drift length 2.2 m which measures up to 21 space points per track; within this lies the inner tracking chamber, a conventional drift chamber which yields up to 8 additional $r\phi$ coordinates; at the centre is a silicon vertex detector of two concentric cylinders of wafers each providing measurements in $r\phi$ and z. The detectors lie within a magnetic solenoid of field 1.5 T, and together give a momentum resolution of $\sigma_{p_\perp}/p_\perp = 0.0006\,(\mathrm{GeV}/c)^{-1} \cdot p_\perp$. The TPC also provides up to 338 measurements of the ionization energy loss of a track from the wires in chambers in the TPC end-plates, as described below.

Data recorded with ALEPH during 1992 were used. Hadronic events were required to have at least five well-reconstructed charged tracks having a total energy of at least 20% of the centre-of-mass energy, where a track must originate from within a cylinder of radius 2 cm and length 10 cm centred on the nominal interaction point, and must have at least four TPC hits, a polar angle in the range $20° < \theta < 160°$ (corresponding to at least 110 wires crossed) and a transverse momentum $p_T > 200\,\mathrm{MeV}/c$. The sphericity axis was required to have a polar angle θ_{sph} in the range $35° < \theta_{sph} < 145°$. A sample of 516 963 events were selected in this way, with a residual contamination from $Z \to \tau^+\tau^-$ determined from Monte Carlo to be 0.3%.

In addition to the cuts described above, several cuts on the quality of the measured ionization were applied. The increase in sample length as polar angle decreases from 90° to 45° leads to a significant improvement in resolution. At smaller angles to the beam axis, tracks pass through the TPC end-plates, with a loss of wire measurements and a consequent degradation in resolution. Therefore tracks were required to have a polar angle such that $0.25 < |\cos\theta| < 0.85$. At least 150 wire measurements were required, or at least 80 wire measurements for scaled momentum $z < 0.018$ (when the track may spiral within the TPC). Tracks at high momentum (the relativistic rise region) with $dE/dx > 2.3$, arising from false association of ionization from distinct tracks, were excluded, where dE/dx is the truncated mean ionization, to be described in the following section. Nuclear interactions in the material of the detector give rise to an excess of protons over antiprotons at low momentum. Due to the difficulties of simulating the rates of these interactions, only negative tracks were selected for $z < 0.060$.

3 $\frac{dE}{dx}$ measurement

Charged particles are identified by a simultaneous measurement of their momentum p and ionization energy loss in the TPC. The ionization deposited by a track traversing the entire TPC is sampled on up to 338 sense wires, of pitch 4 mm, in multiwire proportional chambers, of which there are 18 at each end of the detector. The TPC operates with a gas pressure at slightly above atmospheric pressure, and follows atmospheric variations. A correction is made for the resulting change in the gas amplification factor. The raw charge measurements are corrected for geometrical path length, charge attenuation along the drift length, variations in gain over the surface of a sector and variations between sectors.

An individual charge sample is associated with a track if it lies within a window in z (the drift direction) of ± 29 mm about the fitted track helix (the FWHM of the distribution of electrons from a track parallel to the end-plate is 14 mm). If the sample lies within 30 mm of another helix, it is rejected. The specific energy loss $\mathrm{d}E/\mathrm{d}x$ is estimated from the truncated mean of the usable samples associated with a track, discarding the lower 8% and upper 40% of samples. The upper cut prevents large fluctuations in the mean from relatively rare high-energy collisions corresponding to the Landau tail of the energy-loss distribution. The 8% cut is necessary because a lower threshold cut on the charge measured per wire is made in the front-end electronics, in order to keep the raw data rate to a manageable level. Tracks nearly perpendicular to the beam have a shorter sample length, and hence a smaller absolute charge, per wire, so that individual samples are more likely to be rejected by the threshold cut and the measured $\mathrm{d}E/\mathrm{d}x$ is shifted upwards. The fraction of wire measurements below threshold is practically never larger than 8%, so removing the lower 8% of samples (including those already below threshold) eliminates any threshold bias. The 1.5 T magnetic field causes low-momentum particles to spiral within the TPC. Only the first half-turn of the helix is used to estimate $\mathrm{d}E/\mathrm{d}x$, hence the maximum number of samples available is reduced for these tracks.

In a scatter-plot of $\mathrm{d}E/\mathrm{d}x$ versus momentum p for tracks from hadronic events (figure 1a), clearly-defined bands corresponding to electrons, pions, kaons and protons can be seen (muons cannot be distinguished from the pions). The $\mathrm{d}E/\mathrm{d}x$ is normalized such that minimum-ionizing pions have $<\mathrm{d}E/\mathrm{d}x> \equiv 1$. The large statistical spread in $\mathrm{d}E/\mathrm{d}x$ means that the bands overlap over a significant range of momentum — the separation between kaons and protons is less than two standard deviations for momenta greater than 3 GeV/c. Hence the particle rates can be determined on a statistical basis only. In those regions where bands of different species cross, their rates cannot be determined.

The expected energy loss per unit length, $<\mathrm{d}E/\mathrm{d}x>=\mu$, where $\mathrm{d}E/\mathrm{d}x$ is the truncated mean, is given by the Bethe–Bloch formula [5], a parametrization of which has been fitted to ALEPH data: protons and kaons in the $\frac{1}{\beta^2}$ region, pions at the minimum and conversion electrons in the Fermi plateau from hadronic events, together with isolated electrons and muons from $\mathrm{Z} \to \ell^+\ell^-$ at the extreme of the plateau [6]. Residual deviations of this parametrization from the data at given $\beta\gamma$, of order 0.5% (equivalent to $\sim 0.07\sigma$), were accounted for by refitting the pion peak position in bins of scaled momentum. The expected $\mathrm{d}E/\mathrm{d}x$ as a function of momentum is superimposed on figure 1a.

The truncated mean for tracks of given polar angle and number of individual charge measurements n_s is expected to follow a Gaussian distribution with mean μ. The width $\sigma_{dE/dx}$ depends on n_s, and on the path length of the individual measurements. The resolution was measured with a sample of minimum-ionizing pions, which are both abundant and well-separated from other particle bands. The resolution is parametrized as

$$\frac{\sigma_{dE/dx}}{\mu} = \frac{0.85}{n_s^{c_1}\ell^{c_2}\mu^{c_3}}.$$

Here, ℓ is the mean length of all the usable measurements and $c_{1,2,3} \approx \frac{1}{2}$ are constants [6]. The factors $\sim \ell^{-\frac{1}{2}}$ and $\mu^{-\frac{1}{2}}$ arise because the number n of primary electrons (after truncation) follows a Poisson distribution with mean proportional to $\ell\mu$; fluctuations in n are then expected to be of order $\sqrt{n}$. For a minimum ionizing track with 270 samples and a mean sample length of 0.5 cm the resolution is 7.0%.

Hence the dE/dx distribution for all the selected tracks is a sum of many Gaussians of a single mean μ but with varying widths $\sigma_{dE/dx}(n_s, \ell)$. Figure 1b shows the difference between the measured and expected dE/dx for a sample of minimum-ionizing pions in units of the resolution: the measured dE/dx is well described by a single Gaussian over three standard deviations.

4 Likelihood fit for the particle rates

The differential cross-sections for $\pi^{\pm}$, $K^{\pm}$ and $(p, \bar{p})$ were determined by a maximum-likelihood fit to the measured dE/dx distribution in 48 bins in $z = p_{\rm hadron}/p_{\rm beam}$. For a given momentum, number of wire measurements and mean sample length, the distribution of dE/dx is given by the probability density

$$g(\tfrac{dE}{dx}, n_s, \ell; f_i) = \sum_i \frac{f_i}{\sqrt{2\pi}\sigma_i} \exp\left(\frac{-\left(\frac{dE}{dx} - \mu_i\,(p)\right)^2}{2\sigma_i^2}\right)$$

where μ_i is the expected dE/dx and f_i is the fraction of particles of type $i = e$, π, K or p (*i.e.* a sum of four Gaussians: muons are not distinguished in the fit, but are removed in the efficiency correction). Here, σ_i includes the dE/dx resolution $\sigma_{dE/dx}$ and the uncertainty in μ_i from the error on momentum p. One of the f_i is determined by the constraint $\sum_i f_i = 1$. The fractions are obtained by maximizing the function

$$\mathcal{L} = \frac{e^{-\varphi}\varphi^N}{N!} \prod_{j=1}^{N} g_j\,(\tfrac{dE}{dx}, n_s, \ell; f_i)$$

where the product runs over all the tracks in each z bin. The Poisson factor in front represents the probability of obtaining a sample of size N from a distribution of mean φ. With $\varphi_i = \varphi f_i$ being the mean number of particles of type i, $\mathcal{L}$ becomes

$$\mathcal{L} = \frac{e^{-(\varphi_e+\varphi_\pi+\varphi_K+\varphi_p)}}{N!} \prod_{j=1}^{N} g_j\,(\tfrac{dE}{dx}, n_s, \ell; \varphi_i)$$

There are four free parameters, φ_π, φ_K, φ_p and φ_e, where $\sum_i \varphi_i = \varphi$. All the tracks appear in $\mathcal{L}$ with their correct resolution given their number of charge measurements and polar angle.

Figure 1c shows the dE/dx distribution for $0.12 < z < 0.13$ with the function $g(\frac{dE}{dx}, < n_s >, < \ell >; \varphi_i)$ superimposed, illustrating the quality of the likelihood fit.

5 Background and efficiency corrections

Background contamination of the hadronic event sample and efficiency of the selection cuts were determined by Monte Carlo simulation. The background from $Z \to \tau^+\tau^-$ decays was obtained with a sample of events generated with the KORALZ Monte Carlo [7], and amounts to 0.3% of selected hadronic events. The contamination of individual species is small, due to the low multiplicity of τ events, reaching 2.4% of pions in the highest z bin ($0.6 < z < 0.8$), and was subtracted bin by bin from the φ_i. The background from $\gamma\gamma \to$ hadrons is negligible.

The measured particle rates were then corrected for the effects of geometrical acceptance and track reconstruction efficiency, interactions in the material of the detector and initial state radiation using an event generator based on the DYMU [8] and JETSET 7.3 programs. With a detailed simulation of the detector, the effect of the individual selection cuts was compared in data and Monte Carlo. Good agreement was found, except in the distribution of number of samples per track: high-momentum tracks, which remain close to the core of a jet and are most subject to the loss of samples through overlap with other tracks, have on average slightly fewer wire measurements per track in the Monte Carlo than in the data. A momentum-dependent adjustment was made in the cut on n_s for the Monte Carlo, so that

the same fraction of tracks pass the cut in data and Monte Carlo. This correction varies smoothly with increasing z from 2% up to 10% of tracks in the highest bins, and does not bias the relative proportions of hadrons selected.

A bin-by-bin correction factor was calculated for each species from the Monte Carlo. To allow comparison with other published data, all particles of lifetime less than 10^{-9} s were forced to decay. In consequence, the particle rates include contributions from Λ and other weakly-decaying baryons, and from K^0_S decays, but not from K^0_L or $K^{\pm}$ decays.

The rapid energy loss in the $\frac{1}{\beta^2}$ region causes protons and kaons to slow down significantly in their passage through the detector, so that the reconstructed momentum is systematically lower than the original momentum. This migration to lower momentum has been studied with the Monte Carlo, and a correction applied for kaons of $z < 0.010$ and protons of $z < 0.018$. The acceptance after the cuts described in section 2 (apart from the requirement of negative tracks) is typically $\sim 50\%$ for all species, dipping to $\sim 35\%$ at high momentum where overlapping tracks reduce the number of samples. The acceptance drops rapidly to $\sim 10\%$ for highly ionizing protons and kaons below $0.35\,\mathrm{GeV}/c$, due to saturation of the charge measurement. The contamination in the pion rate from muons, which are not distinguished in the likelihood fit, was corrected according to the prediction of JETSET. The correction is 3.5% at low momentum, decreasing to 2% at $z \sim 0.04$ and then increasing again to 5% at high momentum. A large fraction of low-momentum charged kaons decay in the volume of the TPC. Studies show that decay products of highly-curved, low-momentum tracks are virtually always reconstructed as separate tracks, and are effectively removed by the requirement that tracks originate near the interaction point.

6 Systematic error analysis

The fitted particle rates depend crucially on the expected $\mathrm{d}E/\mathrm{d}x$, μ, and resolution, $\sigma_{\mathrm{d}E/\mathrm{d}x}$, entered in the likelihood function. After the corrections to the raw charge measurements described in section 3, some residual systematic variations in $<\mathrm{d}E/\mathrm{d}x>$ are observed. Minimum-ionizing pions exhibit a $\pm 0.3\%$ variation in mean measured $\mathrm{d}E/\mathrm{d}x$ with polar angle, and a relative deviation of up to $\pm 3\%$ from the expected resolution.

The systematic error in the particle rates arising from this uncertainty in μ was estimated by shifting μ_i by 0.3% for a single species and repeating the likelihood fit. This leads to errors of $\sim 1\%$, 6% and 8% in the rates of π, K and p respectively in the relativistic rise. Near the cross-over region the errors are larger, reflecting the ambiguity in the $\mathrm{d}E/\mathrm{d}x$ of different species. Non-Gaussian tails in the $\mathrm{d}E/\mathrm{d}x$ distribution give an error approximately one tenth of this. Likewise the error due to the uncertainty in $\sigma_{\mathrm{d}E/\mathrm{d}x}$ was estimated by scaling $\sigma_{\mathrm{d}E/\mathrm{d}x}$ and repeating the fit: errors of $\sim 0.4\%$, 0.4% and 2.5% result in the relativistic rise. These errors are highly correlated in consecutive bins, and between species within a bin.

Nuclear interactions in the material of the detector give rise to an excess of protons over antiprotons at low momentum. Comparison of this excess in Monte Carlo and data, and of the distributions of tracks not originating from the interaction point, indicate an uncertainty in the rate of particles produced in nuclear interactions of up to $\pm 10\%$. This leads to an uncertainty of $\sim 0.1\%$, 0.03% and 0.2% for π, K and p respectively (recall that only negative tracks are selected for $z < 0.060$).

As described above, the cut on n_s was adjusted in the Monte Carlo such that the same fraction of tracks pass the cut as in the data. The relative change in efficiency obtained from the Monte Carlo is the same for all species in the relativistic rise. An error of 3% (the typical size of the correction) on the number of selected particles was assigned for all species. For highly-ionizing kaons below $z = 0.010$, and protons below $z = 0.018$, the error is 5%.

The individual error contributions are added in quadrature. The largest contribution for pions is the 3% uncertainy in the efficiency. For protons and kaons in the relativistic rise the largest error arises from the uncertainty in the expected $\mathrm{d}E/\mathrm{d}x$, μ; at low z statistical errors and the error on the efficiency dominate.

7 Results

In figures 2–4 the differential cross-sections

$$\frac{1}{\sigma_T}\frac{\mathrm{d}\sigma}{\mathrm{d}z}\,(\mathrm{Z}\to i+X)$$

are shown for $i=\pi^{\pm}$, $\mathrm{K}^{\pm}$ and $(\mathrm{p},\bar{\mathrm{p}})$. Here σ_T is the total cross-section for the process $\mathrm{Z}\to$ hadrons, $z=p/p_{beam}$ is the scaled momentum. There is fair agreement within errors with the pion and kaon spectra measured by OPAL. The proton spectra are in agreement at low z, but OPAL observes fewer protons for $z>0.1$. Also shown are the predictions of the JETSET 7.3 and HERWIG 5.6 Monte Carlos. The fragmentation parameters of both models have been tuned to reproduce global event-shape and charged-particle inclusive distributions [9]. There is reasonable agreement in the $\pi^{\pm}$ differential cross-section. Both models predict a softer $\mathrm{K}^{\pm}$ spectrum than is observed. Neither model reproduces the proton spectrum. Some problems may arise due to the inadequate simulation of the decays of b and c hadrons, and differences between models may be partly attributed to this. The ALEPH program HVFL04 [10] applies a more sophisticated description of these decays to JETSET only. The results are listed in tables 1–3. The individual contributions to the overall error are shown separately.

In figure 5 the ratios of the rates of kaons to pions and protons to pions are shown as a function of z, together with the Monte Carlo predictions. With the parameter values of reference [9], the ratio of strange to non-strange mesons is underestimated by both models above $z=0.2$, and neither reproduces the fraction of protons as a function of z.

An important property of perturbative QCD is the coherence of gluon radiation. Destructive interference reduces the phase space for soft gluon emission leading to a suppression of gluons at low z. The $\xi=\ln(1/z)$ distribution for gluons can be calculated in the modified leading logarithm approximation (MLLA), in which dominant leading and next-to-leading order terms at each branching are resummed to all orders. This is equivalent to a parton shower including coherence. The distribution is asymptotically Gaussian about its peak [11] with a maximum at

$$\xi^{\star}=Y\left(\frac{1}{2}+a\sqrt{\frac{\alpha_s(Y)}{32N_c\pi}}-a^2\frac{\alpha_s(Y)}{32N_c\pi}+\cdots\right) \qquad (1)$$

where $Y=\ln\left(E_{cm}/2\Lambda\right)$, $\alpha_s(Y)=2\pi/bY$, $a=\left(11N_c+2n_f/N_c^2\right)/3$ and $b=\left(11N_c-2n_f\right)/3$ for N_c colours and n_f flavours. Three flavours are assumed, as the three light quark species dominate quark pair production in the gluon cascade. Λ is an effective QCD scale, not directly related to $\Lambda_{\overline{\mathrm{MS}}}$. The leading term $\xi^{\star}=\frac{1}{2}Y$ arises from the so-called double logarithm approximation in which only simultaneously soft and collinear divergent terms are resummed. Equation (1) can be compared to a parton shower without angular ordering [11], for which $\xi^{\star}=Y$, a factor two greater than expected with coherence.

According to the hypothesis of local parton-hadron duality [11], the inclusive distributions of final-state hadrons should have the same form, up to a normalization constant. Hence, $\xi^{\star}$ should vary as a function of $\ln(E_{cm})$ according to equation (1), with a single free parameter Λ. The value of Λ can be expected to change with particle type.

Peak positions $\xi^{\star}$ for the inclusive differential cross-sections presented here were determined by fitting a Gaussian about the maximum in $\mathrm{d}\sigma/\mathrm{d}\xi$. At extreme values of ξ, the Gaussian approximation is no longer expected to be valid. Therefore the fitted range was gradually extended until the χ^2 per degree of freedom began to increase rapidly; the maximum range over which the χ^2 per degree of freedom had remained flat gave the nominal $\xi^{\star}$. When the fitted $\xi^{\star}$ for subsets of this range varied by more than the expected statistical fluctuation, a systematic error was determined, taking into account the correlation between the measurements. Figure 6 shows the differential cross-section in ξ with the fits superimposed.

The effect of systematic errors in the cross-section measurements was estimated by moving the data by their individual systematic errors and refitting over the same range. The systematic errors were

conservatively assumed to be completely correlated from bin to bin, but to be anticorrelated on either side of the peak. The fitted $\xi^\star$ and their errors are shown in table 4. The same technique was applied to the inclusive differential cross-sections for K^0_s and Λ baryons [12]. The resulting $\xi^\star$ are shown in table 4.

The stability of the fits, given the lack of data on the peak, was studied in the corresponding distributions for charged particles (without identification) [9], K^0_s and Λ baryons, for which data are available across the entire ξ range. Including and excluding from the fit data corresponding to the unmeasured regions in the respective $\pi^\pm$, $K^\pm$ and $(p, \bar{p})$ distributions, the fitted peak was found to move by much less than the quoted error.

Peak positions for pions, kaons and protons have been published by OPAL [3] at the Z and TOPAZ [13] at 58 GeV/c. Differential cross-sections published by TASSO [14, 15] (14–44 GeV/c) and TPC [16, 17] (29 GeV/c) quote a combined statistical and systematic error. For these data a peak position was determined as described above, assuming the quoted errors to be uncorrelated. Variations in $\xi^\star$ resulting from changing the range fitted in ξ are within the statistical error. Figure 7 shows the fitted $\xi^\star$ as a function of energy. The error shown is the quadratic sum of statistical and systematic errors.

Superimposed on figure 7 are fits according to equation (1). For both pions and protons there is good agreement with the MLLA calculation. The kaon $\xi^\star$ at the Z are low relative to this calculation and the lower energy data, and are excluded from the fit. Kaons arising from the decays of b hadrons lie just to the left of the peak in ξ with respect to kaons created from quarks in fragmentation, pulling $\xi^\star$ to lower values. It is estimated that the larger proportion of $b\bar{b}$ pairs produced at the Z relative to e^+e^- annihilation at lower energies causes $\xi^\star$ to move downwards by ~ 0.25. This shift is shown on figure 7, and brings the data into reasonable agreement with an extrapolation of the fitted function. Also shown for pions on figure 7, and clearly incompatible with the data, is the predicted dependence $\xi^\star = Y$ of an incoherent shower.

8 Conclusion

Inclusive differential cross-sections for $\pi^\pm$, $K^\pm$ and $(p, \bar{p})$ in hadronic Z decays have been measured as a function of $z = p_{\mathrm{hadron}}/p_{\mathrm{beam}}$ There is fair agreement with the measurement of OPAL in the pion and kaon differential cross-sections; we observe a harder proton spectrum, however. With the parameter values of reference [9], JETSET 7.3 and HERWIG 5.6 predict a softer $K^\pm$ spectrum than is observed, and neither reproduces the measured proton differential cross-section. The evolution with centre-of-mass energy of the peak position $\xi^\star$ has been determined, and is found to be in good agreement with the MLLA calculation, which incorporates the coherence of gluon radiation. An incoherent parton shower is incompatible with the data.

9 Acknowledgements

It is a pleasure to thank our colleagues in the accelerator divisions of CERN for the excellent performance of LEP. Thanks are also due to the technical personnel of the collaborating institutions for their support in constructing and maintaining the ALEPH experiment. Those of us from non-member states thank CERN for its hospitality.

References

[1] T. Sjöstrand and M. Bengtsson, Computer Phys. Commun. **43** (1987) 367.

[2] G. Marchesini, B. R. Webber, G. Abbiendi, I. G. Knowles, M. H. Seymour and L. Stanco, Computer Phys. Commun. **67** (1992) 465.

[3] R. Akers *et al.* (OPAL Collab.), CERN-PPE/94-049, submitted to Zeitschrift für Physik.

[4] D. Decamp *et al.* (ALEPH Collab.), Nucl. Instr. and Meth. A **294** (1990) 121.

[5] H. A. Bethe, Ann. Physik **5** (1930) 325.
F. Bloch, Z. Phys. **81** (1933) 363.

[6] W. B. Atwood *et al.*, Nucl. Instr. and Meth. A **306** (1991) 446.

[7] S. Jadach, J. H. Kühn and Z. Wąs, Comp. Phys. Comm. **64** (1991) 275.
S. Jadach, B. F. L. Ward and Z. Wąs, Comp. Phys. Comm. **66** (1991) 276.

[8] J. E. Campagne and R. Zitoun, Z. Phys. C **43** (1989) 469.

[9] D. Busculic *et al.* (ALEPH Collab.), Z. Phys. C **55** (1992) 209.

[10] D. Busculic *et al.* (ALEPH Collab.), Z. Phys. C **62** (1994) 179.

[11] Yu. L. Dokshitzer, V. A. Khoze, A. H. Mueller and S. I. Troyan, Basics of Perturbative QCD, Editions Frontieres, 1991 (and references therein).

[12] D. Busculic *et al.* (ALEPH Collab.), CERN-PPE/94-074, submitted to Zeitschrift für Physik.

[13] R. Itoh: Talk given at the Int. Lepton-Photon Symposium and Europhysics Conference on High Energy Physics, World Scientific, Geneva, 1991.

[14] M. Althoff *et al.* (TASSO Collab.), Z. Phys. C **17** (1983) 5.

[15] W. Braunschweig *et al.* (TASSO Collab.), Z. Phys. C **42** (1989) 189.

[16] H. Aihara *et al.* (TPC Collab.), Phys. Rev. Lett. **61** (1988) 1263.

[17] G. D. Cowan, University of California, LBL-24715 (1988).

$\pi^{\pm}$				
z interval	$<z>$	$\frac{1}{\sigma_T}\frac{d\sigma}{dz}$	$\pm\sigma_{\rm stat}$	$\pm\sigma_{\rm sys}$
0.0050-0.0055	0.00526	482.9	$\pm$ 5.9	$\pm$ 1.3
0.0055-0.0060	0.00574	462.6	$\pm$ 4.8	$\pm$ 0.9
0.0060-0.0065	0.00622	496.5	$\pm$ 4.6	$\pm$ 0.8
0.0065-0.0070	0.00673	511.2	$\pm$ 4.4	$\pm$ 0.8
0.0070-0.0075	0.00722	507.7	$\pm$ 4.2	$\pm$ 0.7
0.0075-0.0080	0.00773	538.5	$\pm$ 4.4	$\pm$ 0.7
0.0080-0.0085	0.00822	484.2	$\pm$ 3.9	$\pm$ 0.6
0.0085-0.0090	0.00871	499.7	$\pm$ 3.9	$\pm$ 0.7
0.0090-0.0095	0.00922	494.6	$\pm$ 3.8	$\pm$ 0.6
0.0095-0.010	0.00972	473.9	$\pm$ 3.6	$\pm$ 0.5
0.010-0.011	0.0105	460.9	$\pm$ 2.5	$\pm$ 0.5
0.011-0.012	0.0115	425.6	$\pm$ 2.3	$\pm$ 0.5
0.012-0.013	0.0125	420.7	$\pm$ 2.3	$\pm$ 0.4
0.013-0.014	0.0135	380.5	$\pm$ 2.2	$\pm$ 0.4
0.014-0.016	0.0147	360.8	$\pm$ 1.5	$\pm$ 0.6
0.016-0.018	0.0167	324.0	$\pm$ 1.4	$\pm$ 1.8
0.045-0.050	0.0470	103.96	$\pm$ 0.61	$\pm$ 2.09
0.050-0.055	0.0520	89.95	$\pm$ 0.53	$\pm$ 1.02
0.055-0.060	0.0570	78.96	$\pm$ 0.50	$\pm$ 0.90
0.060-0.065	0.0619	69.36	$\pm$ 0.35	$\pm$ 0.72
0.065-0.070	0.0669	61.35	$\pm$ 0.33	$\pm$ 0.60
0.070-0.075	0.0719	55.27	$\pm$ 0.32	$\pm$ 0.49
0.075-0.080	0.0769	49.91	$\pm$ 0.30	$\pm$ 0.44
0.080-0.085	0.0819	44.33	$\pm$ 0.29	$\pm$ 0.38
0.085-0.090	0.0870	40.24	$\pm$ 0.27	$\pm$ 0.34
0.090-0.10	0.0942	35.38	$\pm$ 0.18	$\pm$ 0.30
0.10-0.11	0.104	29.51	$\pm$ 0.17	$\pm$ 0.25
0.11-0.12	0.114	24.91	$\pm$ 0.16	$\pm$ 0.22
0.12-0.13	0.124	21.06	$\pm$ 0.14	$\pm$ 0.18
0.13-0.14	0.134	18.16	$\pm$ 0.13	$\pm$ 0.16
0.14-0.15	0.144	15.46	$\pm$ 0.12	$\pm$ 0.15
0.15-0.16	0.154	13.64	$\pm$ 0.12	$\pm$ 0.13
0.16-0.18	0.169	11.00	$\pm$ 0.07	$\pm$ 0.11
0.18-0.20	0.189	8.484	$\pm$ 0.066	$\pm$ 0.094
0.20-0.25	0.222	5.621	$\pm$ 0.035	$\pm$ 0.071
0.25-0.30	0.272	3.181	$\pm$ 0.026	$\pm$ 0.047
0.30-0.40	0.342	1.563	$\pm$ 0.013	$\pm$ 0.028
0.40-0.60	0.476	0.4495	$\pm$ 0.0051	$\pm$ 0.0100
0.60-0.80	0.674	0.0767	$\pm$ 0.0021	$\pm$ 0.0021

Table 1: Differential cross-section $\frac{1}{\sigma_T}\frac{d\sigma}{dz}$ as a function of $z = p_{\rm hadron}/p_{\rm beam}$ for $\pi^{\pm}$. The first error shown is the statistical error. The second includes the systematic errors from the uncertainties in μ (dominant for $z > 0.045$) and $\sigma_{dE/dx}$ and from nuclear interactions. There is an additional 3% relative error from the uncertainty in the n_s distribution.

$K^{\pm}$				
z interval	$<z>$	$\frac{1}{\sigma_T}\frac{d\sigma}{dz}$	$\pm\sigma_{stat}$	$\pm\sigma_{sys}$
0.0055-0.0060	0.00574	12.40	± 1.12	± 0.01
0.0060-0.0065	0.00622	13.27	± 0.91	± 0.01
0.0065-0.0070	0.00673	15.33	± 0.90	± 0.01
0.0070-0.0075	0.00722	17.43	± 0.92	± 0.02
0.0075-0.0080	0.00773	18.33	± 0.88	± 0.02
0.0080-0.0085	0.00822	19.62	± 0.90	± 0.02
0.0085-0.0090	0.00871	20.02	± 0.86	± 0.05
0.0090-0.0095	0.00922	21.66	± 0.88	± 0.12
0.013-0.014	0.0135	25.84	± 0.66	± 0.50
0.014-0.016	0.0147	27.46	± 0.47	± 0.68
0.016-0.018	0.0167	27.63	± 0.53	± 2.20
0.070-0.075	0.0719	10.60	± 0.30	± 1.28
0.075-0.080	0.0769	9.53	± 0.26	± 0.98
0.080-0.085	0.0819	9.15	± 0.23	± 0.83
0.085-0.090	0.0870	8.41	± 0.21	± 0.71
0.090-0.10	0.0942	7.96	± 0.14	± 0.56
0.10-0.11	0.104	7.26	± 0.13	± 0.47
0.11-0.12	0.114	6.34	± 0.11	± 0.37
0.12-0.13	0.124	5.63	± 0.11	± 0.32
0.13-0.14	0.134	4.94	± 0.10	± 0.28
0.14-0.15	0.144	4.39	± 0.09	± 0.24
0.15-0.16	0.154	4.22	± 0.09	± 0.22
0.16-0.18	0.169	3.63	± 0.06	± 0.18
0.18-0.20	0.189	3.10	± 0.05	± 0.15
0.20-0.25	0.222	2.245	± 0.029	± 0.109
0.25-0.30	0.272	1.538	± 0.025	± 0.076
0.30-0.40	0.342	0.841	± 0.013	± 0.043
0.40-0.60	0.476	0.2936	± 0.0053	± 0.0146
0.60-0.80	0.674	0.0596	± 0.0022	± 0.0031

Table 2: Differential cross-section $\frac{1}{\sigma_T}\frac{d\sigma}{dz}$ as a function of $z = p_{hadron}/p_{beam}$ for $K^{\pm}$. The first error shown is the statistical error. The second includes the systematic errors from the uncertainties in μ (dominant for $z > 0.045$) and $\sigma_{dE/dx}$ and from nuclear interactions. There is an additional 3% relative error (5% below $z = 0.010$) from the uncertainty in the n_s distribution.

$(\mathrm{p}, \bar{\mathrm{p}})$				
z interval	$<z>$	$\frac{1}{\sigma_T}\frac{\mathrm{d}\sigma}{\mathrm{d}z}$	$\pm\sigma_{\mathrm{stat}}$	$\pm\sigma_{\mathrm{sys}}$
0.010-0.011	0.0105	8.32	$\pm$ 0.35	$\pm$ 0.00
0.011-0.012	0.0115	8.95	$\pm$ 0.36	$\pm$ 0.00
0.012-0.013	0.0125	9.80	$\pm$ 0.36	$\pm$ 0.01
0.013-0.014	0.0135	10.30	$\pm$ 0.38	$\pm$ 0.01
0.014-0.016	0.0147	10.70	$\pm$ 0.26	$\pm$ 0.01
0.016-0.018	0.0167	11.58	$\pm$ 0.27	$\pm$ 0.04
0.024-0.026	0.0247	12.37	$\pm$ 0.18	$\pm$ 0.23
0.026-0.028	0.0268	12.46	$\pm$ 0.18	$\pm$ 0.44
0.070-0.075	0.0719	5.315	$\pm$ 0.216	$\pm$ 0.876
0.075-0.080	0.0769	5.008	$\pm$ 0.183	$\pm$ 0.639
0.080-0.085	0.0819	4.445	$\pm$ 0.162	$\pm$ 0.549
0.085-0.090	0.0870	4.555	$\pm$ 0.154	$\pm$ 0.474
0.090-0.10	0.0942	3.742	$\pm$ 0.092	$\pm$ 0.355
0.10-0.11	0.104	3.355	$\pm$ 0.084	$\pm$ 0.292
0.11-0.12	0.114	2.905	$\pm$ 0.077	$\pm$ 0.232
0.12-0.13	0.124	2.653	$\pm$ 0.072	$\pm$ 0.205
0.13-0.14	0.134	2.371	$\pm$ 0.068	$\pm$ 0.178
0.14-0.15	0.144	2.137	$\pm$ 0.064	$\pm$ 0.162
0.15-0.16	0.154	1.878	$\pm$ 0.061	$\pm$ 0.146
0.16-0.18	0.169	1.696	$\pm$ 0.041	$\pm$ 0.118
0.18-0.20	0.189	1.299	$\pm$ 0.036	$\pm$ 0.099
0.20-0.25	0.222	0.966	$\pm$ 0.020	$\pm$ 0.073
0.25-0.30	0.272	0.614	$\pm$ 0.017	$\pm$ 0.054
0.30-0.40	0.342	0.305	$\pm$ 0.009	$\pm$ 0.031
0.40-0.60	0.476	0.0784	$\pm$ 0.0034	$\pm$ 0.0110
0.60-0.80	0.674	0.0054	$\pm$ 0.0011	$\pm$ 0.0022

Table 3: Differential cross-section $\frac{1}{\sigma_T}\frac{\mathrm{d}\sigma}{\mathrm{d}z}$ as a function of $z = p_{\mathrm{hadron}}/p_{\mathrm{beam}}$ for $(\mathrm{p}, \bar{\mathrm{p}})$. The first error shown is the statistical error. The second includes the systematic errors from the uncertainties in μ (dominant for $z > 0.045$) and $\sigma_{\mathrm{d}E/\mathrm{d}x}$ and from nuclear interactions. There is an additional 3% relative error (5% below $z = 0.018$) from the uncertainty in the n_s distribution.

	$\xi^\star$	fitted ξ range
$\pi^\pm$	$3.776 \pm 0.004 \pm 0.024$	1.97–4.77
$\mathrm{K}^\pm$	$2.70 \pm 0.01 \pm 0.09$	1.39–4.34
K^0_s	$2.67 \pm 0.01 \pm 0.05$	1.60–4.40
$(\mathrm{p}, \bar{\mathrm{p}})$	$2.85 \pm 0.01 \pm 0.15$	1.39–3.73
$(\Lambda, \bar{\Lambda})$	$2.72 \pm 0.02 \pm 0.05$	1.20–3.60

Table 4: Position of the peak $\xi^\star$ in $\mathrm{d}\sigma/\mathrm{d}\xi$ for pions, charged and neutral kaons, protons and Λ baryons. The first error quoted is statistical, the second systematic.

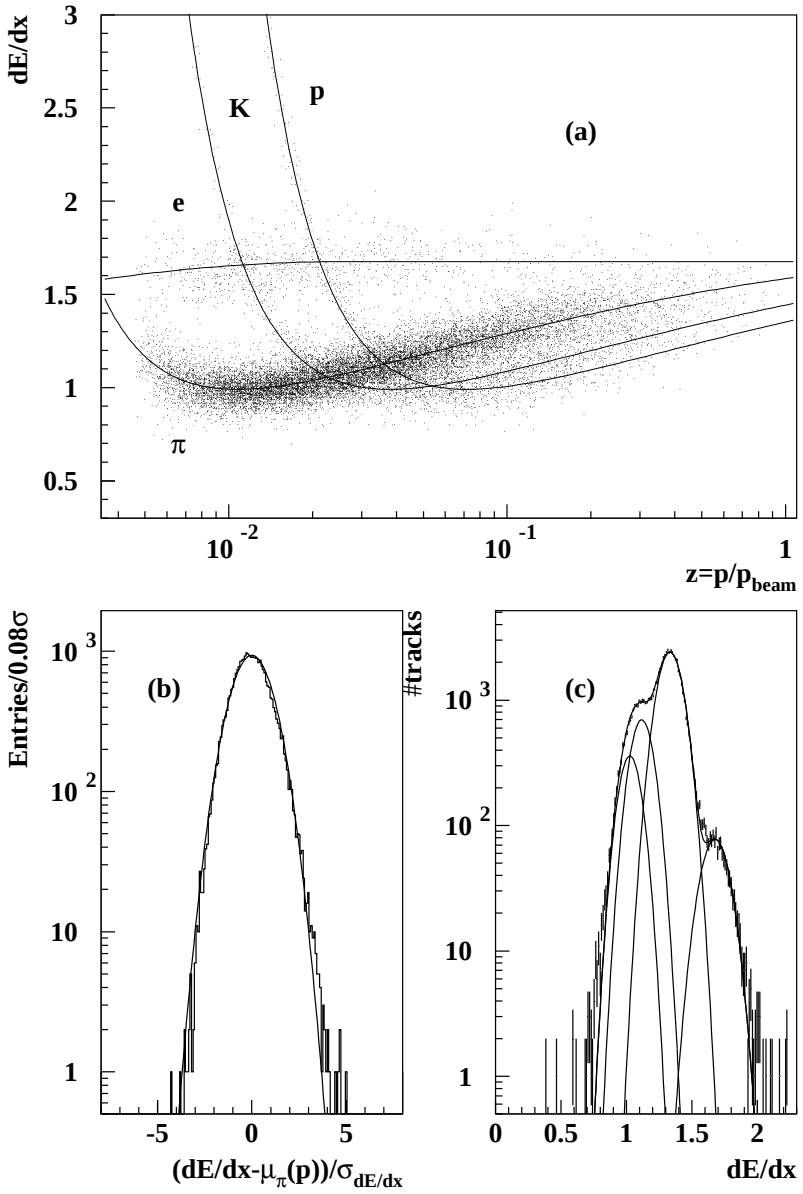


Figure 1: a) Truncated mean $\mathrm{d}E/\mathrm{d}x$ as a function of $z = p/p_{beam}$ for selected tracks from hadronic events.The $\mathrm{d}E/\mathrm{d}x$ is normalized such that minimum-ionizing pions have $<\mathrm{d}E/\mathrm{d}x> \equiv 1$. Superimposed is the expected $\frac{\mathrm{d}E}{\mathrm{d}x}$ for e, π, K and p. b) Measured – expected $\mathrm{d}E/\mathrm{d}x$ in units of the resolution for a sample of minimum-ionizing pions ($0.40 < p < 0.55\,\mathrm{GeV}/c$). Superimposed is a Gaussian of unit width and zero mean. c) Distribution of $\mathrm{d}E/\mathrm{d}x$ for selected tracks in the interval $0.12 < z < 0.13$. Superimposed is an illustration of the likelihood fit.

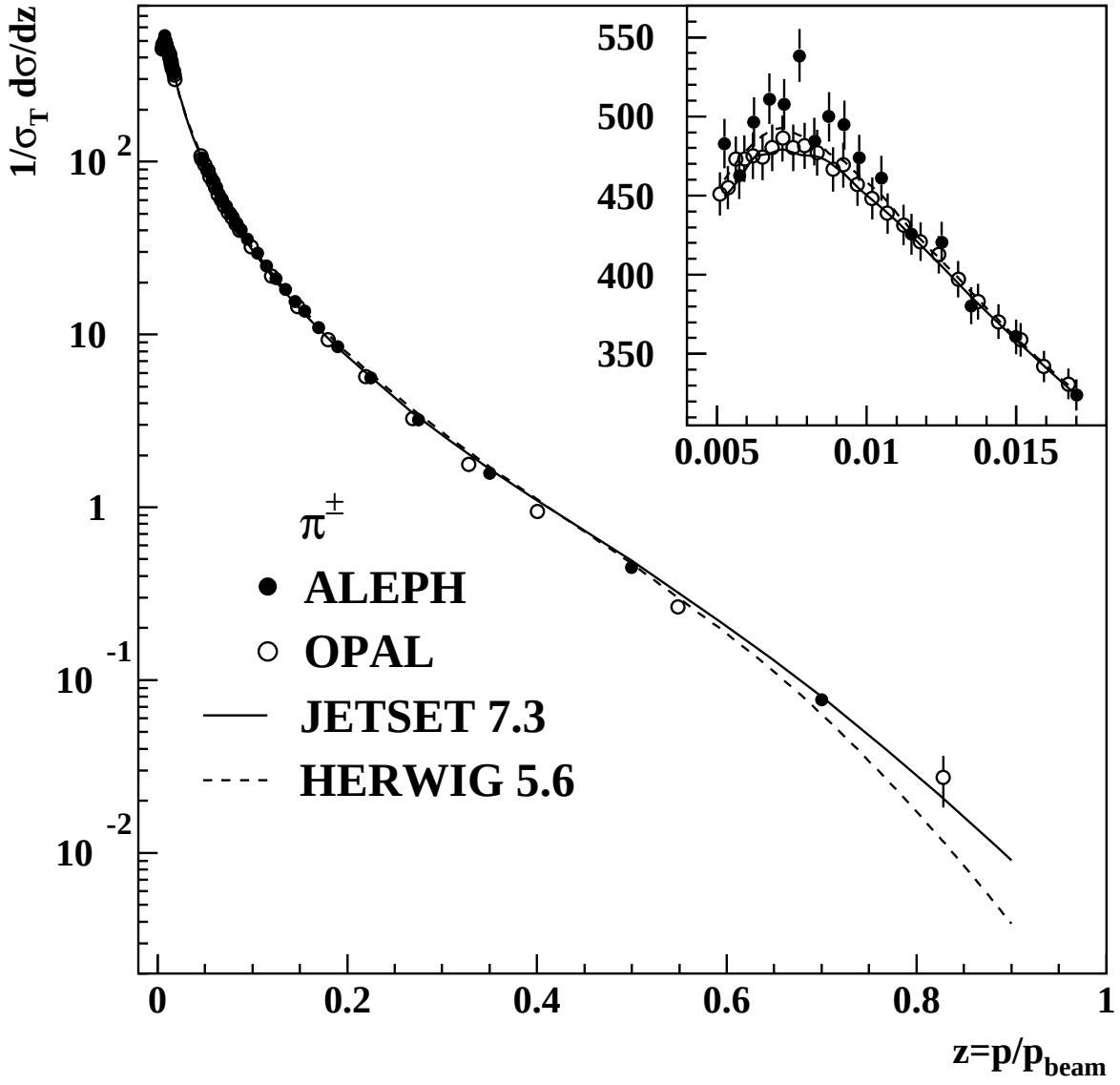


Figure 2: Differential cross-section as a function of $z = p_{\mathrm{hadron}}/p_{\mathrm{beam}}$ for $\pi^{\pm}$, compared with the measurement of OPAL and the predictions of JETSET and HERWIG. The errors shown are the quadratic sum of statistical and systematic errors.

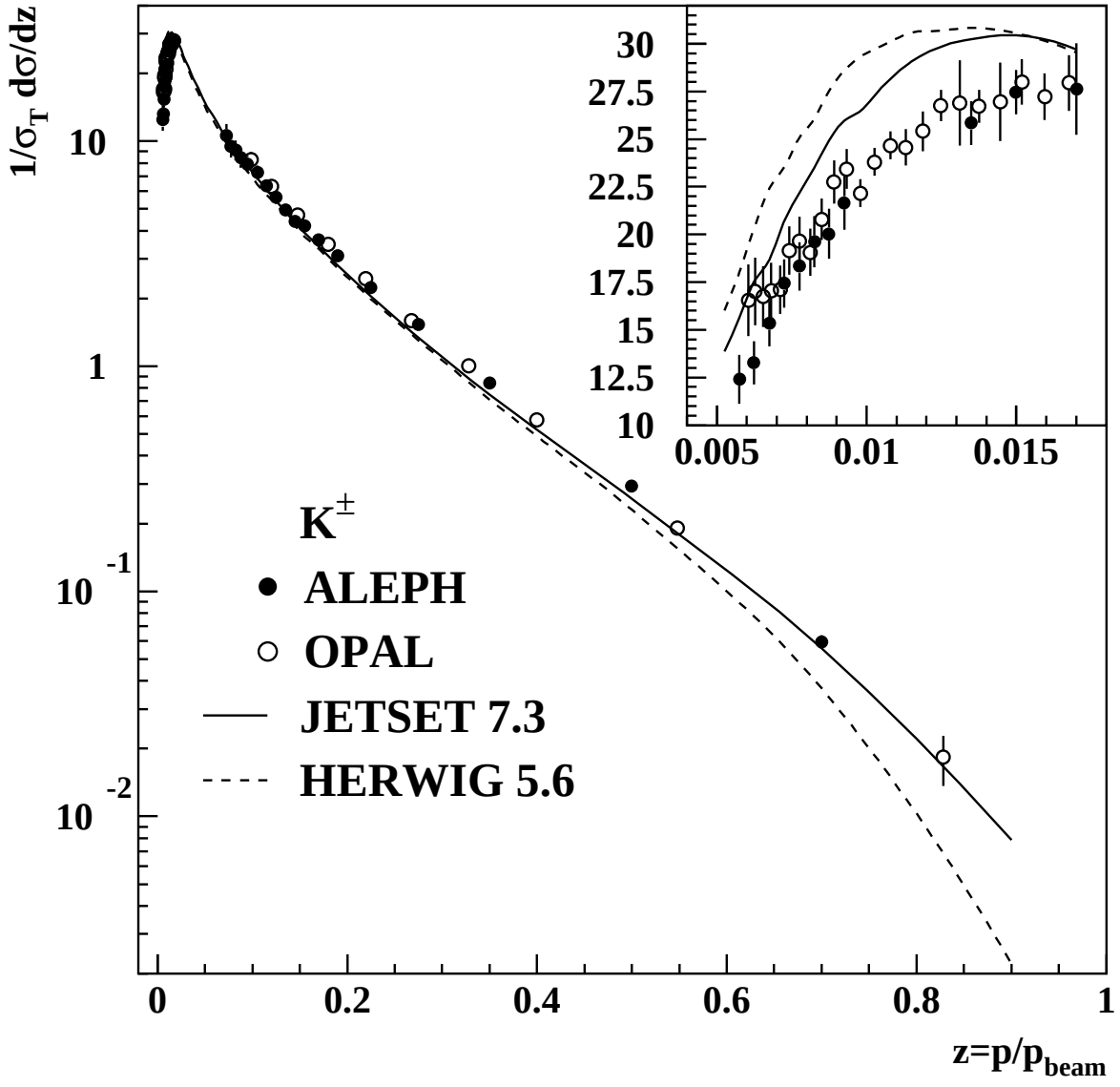


Figure 3: Differential cross-section as a function of $z = p_{\mathrm{hadron}}/p_{\mathrm{beam}}$ for $\mathrm{K}^{\pm}$, compared with the measurement of OPAL and the predictions of JETSET and HERWIG. The errors shown are the quadratic sum of statistical and systematic errors.

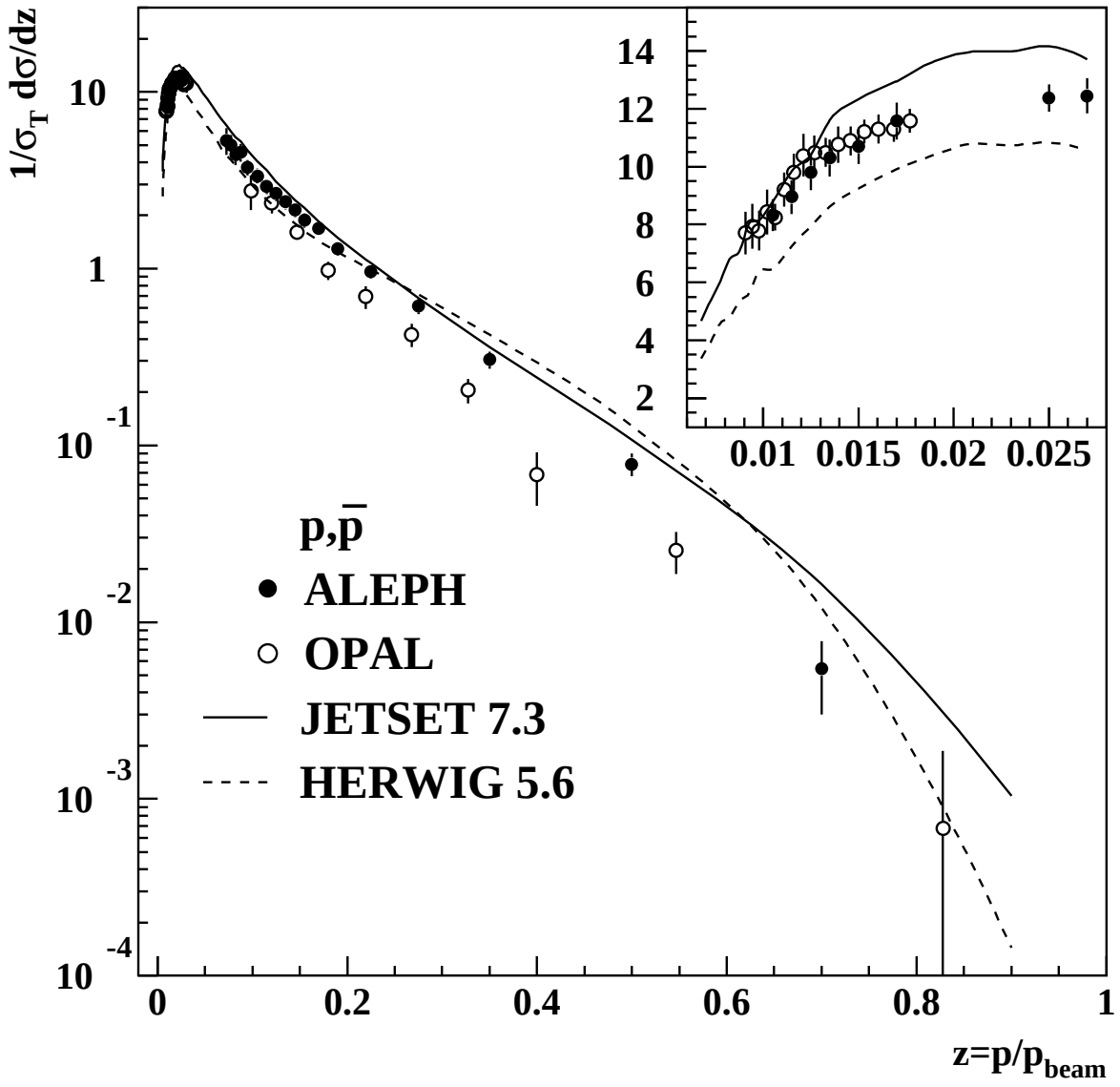


Figure 4: Differential cross-section as a function of $z = p_{\mathrm{hadron}}/p_{\mathrm{beam}}$ for $(\mathrm{p}, \bar{\mathrm{p}})$, compared with the measurement of OPAL and the predictions of JETSET and HERWIG. The errors shown are the quadratic sum of statistical and systematic errors.

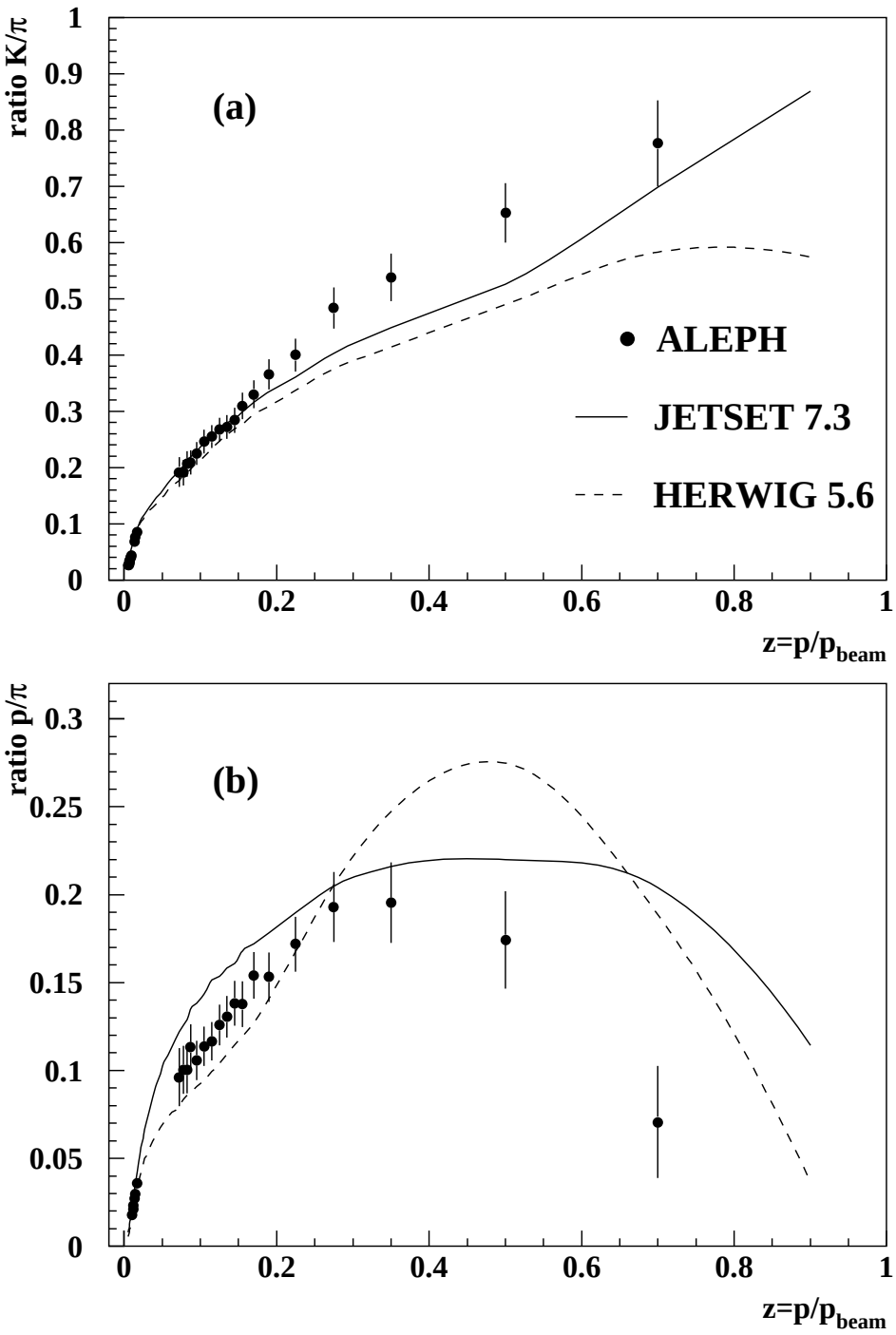


Figure 5: Ratios of the rates of (a) $K^{\pm}/\pi^{\pm}$ and (b) $(p,\bar{p})/\pi^{\pm}$ as a function of $z = p_{\rm hadron}/p_{\rm beam}$, compared with the predictions of JETSET (solid line) and HERWIG (dashed line). The errors shown are the quadratic sum of statistical and systematic errors.

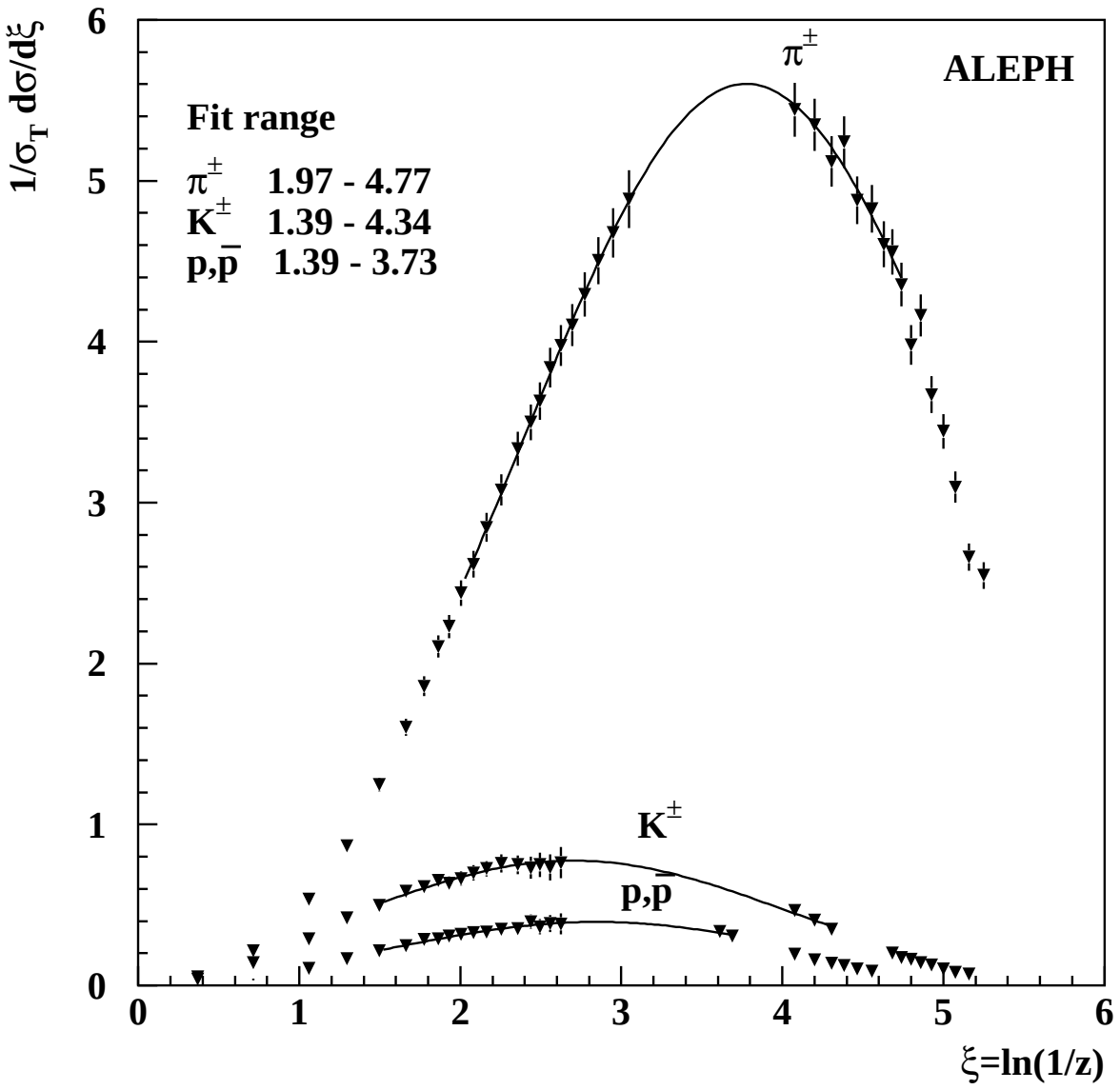


Figure 6: The ξ distribution for $\pi^{\pm}$, $K^{\pm}$ and $(p,\bar{p})$. Superimposed are Gaussian fits around the peak in ξ. The errors shown are a quadratic sum of statistical and systematic errors.

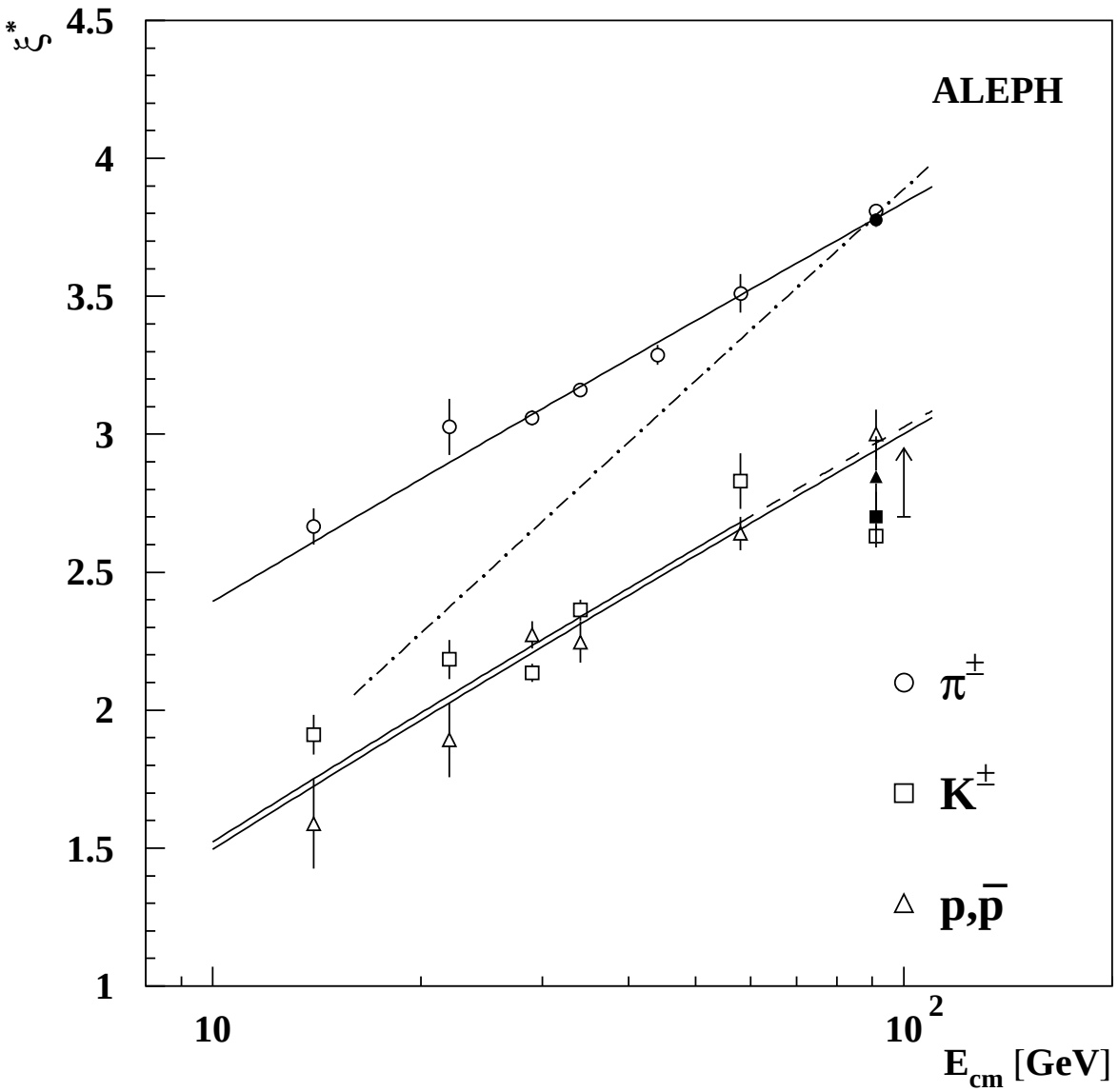


Figure 7: Position of the peak $\xi^\star$ in $\frac{\mathrm{d}\sigma}{\mathrm{d}\xi}$ as a function of centre-of-mass energy for pions, kaons and protons for the inclusive differential cross-sections presented here (filled points) and those of other experiments (TASSO [14,15], TPC/2γ [16,17], TOPAZ [13] and OPAL [3]). The solid lines are fits to, from top to bottom, pion, kaon and proton data according to equation (1), assuming three flavours. The arrow represents the estimated shift in $\xi^\star$ for kaons at the Z due to b hadron decays, and is to be compared with the extrapolation of equation (1) (dashed line). The dot-dashed line is the prediction for an incoherent parton shower.